

Application of a helicity proxy to edge-on galaxies

Axel Brandenburg^{1,2,3,4*} and Ray S. Furuya⁵

¹*Nordita, KTH Royal Institute of Technology and Stockholm University, Roslagstullsbacken 23, SE-10691 Stockholm, Sweden*

²*Department of Astronomy, AlbaNova University Center, Stockholm University, SE-10691 Stockholm, Sweden*

³*JILA and Laboratory for Atmospheric and Space Physics, University of Colorado, Boulder, CO 80303, USA*

⁴*McWilliams Center for Cosmology & Department of Physics, Carnegie Mellon University, Pittsburgh, PA 15213, USA*

⁵*Institute of Liberal Arts and Sciences, Tokushima University, Minami Jousanajima-machi 1-1, Tokushima 770-8502, Japan*

17 March 2020, Revision: 1.63

ABSTRACT

We propose to detect a proxy of the magnetic helicity in galaxies by observing the dust polarization of the edge-on galaxy NGC 891. Our numerical results of mean-field dynamo calculations show that there should be a large-scale component of the rotationally invariant parity-odd B polarization that we predict to be negative in the first and third quadrants, and positive in the second and fourth quadrants. The large-scale parity-even E polarization is predicted to be negative near the axis and positive further away in the outskirts.

Key words: dynamo — MHD — polarization — turbulence — galaxies: magnetic fields — galaxies: individual: NGC 891

1 INTRODUCTION

The magnetic fields of spiral galaxies possess a clear large-scale component along with a fluctuating component of comparable strength (Beck et al. 1996). Owing to the presence of turbulence in the interstellar medium, there is significant turbulent diffusion, which would destroy the large scale magnetic field on a time scale of less than a billion years (Shukurov 1998), unless there is a correspondingly strong anti-diffusive mechanism. The best known mechanism for explaining the origin and maintenance of galactic large-scale magnetic fields is the α effect (Parker 1955; Steenbeck et al. 1966). In the context of galactic dynamo theory, it was first explored by Parker (1971) and Vainshtein & Ruzmaikin (1971). The existence of the α effect requires a violation of statistical mirror symmetry, which implies the presence of magnetic helicity. However, there is no explicit evidence that the α effect really does operate in galaxies.

Methods for measuring the helicity of the magnetic field in our Galaxy and in distant galaxies have been proposed on several occasions in recent years (Volegov & Stepanov 2010; Junklewitz & Enßlin 2011; Oppermann et al. 2011; Brandenburg & Stepanov 2014; Horellou & Fletcher 2014). Measuring this for edge-on galaxies may be particularly advantageous, because we can then see both the upper and lower disc planes simultaneously. However, to measure the magnetic helicity, one needs the full magnetic field vector, but the linear polarization parameters Stokes, Q and U , only allow one to determine the magnetic field direc-

tion up to a 180° ambiguity. For this reason it is preferable to work directly with the Stokes parameters and to determine from them a helicity proxy. The quantity of interest is then the parity-odd contribution to the rotationally invariant constituent of the linear polarization, or possibly the correlation between the parity-even and parity-odd polarizations. This is a relatively new technique, which has recently been applied to the Sun’s magnetic field (Brandenburg et al. 2019; Brandenburg 2019; Prabhu et al. 2020), and was motivated by earlier work in the cosmological context (Kamionkowski et al. 1997; Seljak & Zaldarriaga 1997; Kahnashvili et al. 2014).

In the context of polarimetry of the cosmic microwave background radiation, one commonly decomposes the linear polarization into the parity-even E and the parity-odd B polarizations. They are defined in terms of a global expansion on the full sphere of the sky. Here, however, we are only interested in local Cartesian patches. We can then employ standard Fourier transformation of the complex polarization $P = Q + iU$ to compute the quantity

$$\tilde{R}(k_x, k_z) = (\hat{k}_x - i\hat{k}_z)^2 \int e^{-ik \cdot x} P(x) d^2 x, \quad (1)$$

where a tilde indicates Fourier transformation of a quantity R over the spatial coordinates in the projected plane in the sky, which are here the x and z coordinates. The real and imaginary parts of R give the E and B polarizations, and \hat{k}_x and \hat{k}_z are the x and z components of the planar unit vector $\hat{\mathbf{k}} = \mathbf{k}/k$, with $\mathbf{k} = (k_x, k_z)$ and $k = (k_x^2 + k_z^2)^{1/2}$ being the length of \mathbf{k} . Thus, we have

* E-mail:brandenb@nordita.org

Table 1. Signs of E and B reported in the literature for various cases and viewing directions.

case	E	B	view	reference
rotating convection	–	–	top	Brandenburg et al. (2019)
solar active regions	–	+	top	Prabhu et al. (2020)
Galaxy	–	+	Sun	Brandenburg & Brüggen
spherical dynamo	–	–	side	Brandenburg (2019)
edge-on galaxies	–	–	side	present work

$$E(\mathbf{x}) + iB(\mathbf{x}) \equiv R = \int e^{i\mathbf{k} \cdot \mathbf{x}} \tilde{R}(\mathbf{k}) d^2\mathbf{k} / (2\pi)^2. \quad (2)$$

The occurrence of the factor $(\hat{k}_x - i\hat{k}_z)^2$ is explained in standard text books in the field (Durrer 2008) and reviews Kamionkowski & Kovetz (2016). It should be noted, however, that the signs of both E and B can be defined differently; see Brandenburg (2019) and Prabhu et al. (2020) for a more detailed discussion on the differences. The alternative definition amounts to including a minus sign in Eq. (1), but such a definition is currently only adopted in some studies using spherical geometry (Durrer 2008), where the alternative definition appears more naturally; see Brandenburg (2019). In the following we employ the definition introduced above using Eq. (1).

The E polarization corresponds to cross-like polarization patterns if $E < 0$ and to ring-like patterns if $E > 0$. Positive (negative) B polarizations, on the other hand, correspond to counterclockwise (clockwise) inward spiraling patterns. The latter pattern is evidently parity-odd, because that for $B > 0$ becomes the pattern for $B < 0$ under parity transformation. By contrast, the E patterns do not change under parity transformation. On the other hand, even just the inspection of a pattern from the flipped side of the plane changes the sign of the B polarization, but not that of the E polarization. For this reason, the B polarization can only act as a helicity proxy when one particular viewing direction is physically preferred over the other, which can be the case when the system is inhomogenous, for example rotating convection (Brandenburg et al. 2019).

Even when the system is inhomogenous and a finite B emerges, it is not yet clear what its sign is. This uncertainty may be mainly due to the fact that the B polarization has not yet been studied under sufficiently many circumstances. It does depend on the spatial magnetic field pattern produced by the system. The experience gathered so far is somewhat sketchy; see Table 1 for a summary. The results depend not only on the nature of the physical system under consideration, but also on the viewing direction. Viewing a disk galaxy from the outside, for example edge-on, will produce the opposite result for the B polarization as viewing from the inside, for example when viewing our Galaxy from the position of the Sun, as has been attempted by Brandenburg & Brüggen (2020, in preparation).

Looking at Table 1, there seems to be agreement regarding a negative sign for E , but B can have either sign, depending on circumstances. In rotating convection, $E < 0$ and $B < 0$; see Fig. 10 of Brandenburg et al. (2019). In solar active regions; $E < 0$ but $B > 0$; see Fig. 5 of Prabhu et al. (2020). Also near the Galactic midplane, $E < 0$ and $B >$

0 (Brandenburg & Brüggen, 2020, in preparation). For a spherical mean-field dynamo, Fig. 1 of Brandenburg (2019) shows positive E and B in the north, but this corresponds to $E < 0$ and $B < 0$ after taking his opposite sign definition into account. This would agree with the present paper if we took E near the axis and B in the first and third quadrants in an edge-on view.

The purpose of the present work is to learn more about the theoretically expected patterns for edge-on galaxies. Here, we consider a numerical solution of a simple galactic mean-field dynamo of $\alpha\Omega$ type. The magnetic field is generated by the α effect (Krause & Rädler 1980) and differential rotation. We embed a flat dynamo in a Cartesian domain. We do this by choosing a distribution of α that is concentrated about the midplane and has opposite signs above and below it. The magnetic diffusivity is taken to be constant. The radius of the disc is assumed to be 15 kpc.

2 THE MODEL

We adopt the galactic dynamo model of Brandenburg (2015) and compute an edge-on view of $P = Q + iU$ as

$$P = -\epsilon (b_x + ib_z)^2 / b_{\perp}^2, \quad (3)$$

where $\mathbf{b}_{\perp} \equiv (b_x, b_z)$ is the magnetic field vector in the (x, z) plane and ϵ is the emissivity (Alton et al. 2004; Planck Collaboration Int. XIX 2015), which is here assumed to be constant. The viewing direction is from $y \rightarrow -\infty$, which is consistent with the viewing direction $z \rightarrow \infty$ of (b_x, b_y) , which was applied in rotating convection and inspections of the Sun (Brandenburg et al. 2019). Next, we compute $R = E + iB$ using Eq. (2). We then show $E(x, z)$ and $B(x, z)$ at a given position y ; see Figs. 1 and 2.

We adopt a mean-field model where all dependent variables are defined as azimuthal averages indicated by an overbar. The mean magnetic field $\overline{\mathbf{B}}$ is expressed in terms of the mean magnetic vector potential $\overline{\mathbf{A}}$ as $\overline{\mathbf{B}} = \nabla \times \overline{\mathbf{A}}$. We solve the $\alpha\Omega$ dynamo equation in its simplest form,

$$\frac{\partial \overline{\mathbf{A}}}{\partial t} = \overline{\mathbf{U}} \times \overline{\mathbf{B}} + \boldsymbol{\alpha} \cdot \overline{\mathbf{B}} - \eta_T \mu_0 \overline{\mathbf{J}}, \quad (4)$$

where $\overline{\mathbf{U}}$ is the mean flow, $\overline{\mathbf{J}} = \nabla \times \overline{\mathbf{B}} / \mu_0$ is the mean current density, μ_0 is the vacuum permeability, $\boldsymbol{\alpha} = \text{diag}(\alpha_{\perp}, \alpha_{\perp}, 0)$ is the α tensor in the limit of rapid rotation (Rüdiger 1978), and η_T is the total (microphysical and turbulent) magnetic diffusivity. The mean flow is composed of toroidal and poloidal components, $\overline{\mathbf{U}}_t$ and $\overline{\mathbf{U}}_p$, respectively, describing the galactic rotation profile and a galactic wind.

In the following we assume the galactic rotation to be represented by a modified Brandt rotation profile of the form $\overline{\mathbf{U}}_t = \varpi \Omega(\varpi)$, where $\varpi = (x, y, 0)$ with $\varpi = |\varpi|$ being the cylindrical radius, and

$$\Omega = \Omega_0 / [1 + (\varpi / \varpi_{\Omega})^n]^{1/n} \quad (5)$$

is the angular velocity with $\Omega_0 = 100 \text{ ks}^{-1}$ characterizing the rigid rotation law for $\varpi < \varpi_{\Omega}$ and $\varpi_{\Omega} = 3 \text{ kpc}$ is the radius where the rotation law attains constant linear velocity with $V_0 = \Omega_0 \varpi_{\Omega} \approx 300 \text{ km s}^{-1}$. The exponent $n = 4$ has been chosen to make the transition from rigid to constant rotation sharp.

For the α effect we assume a nonlinear (α -quenched)

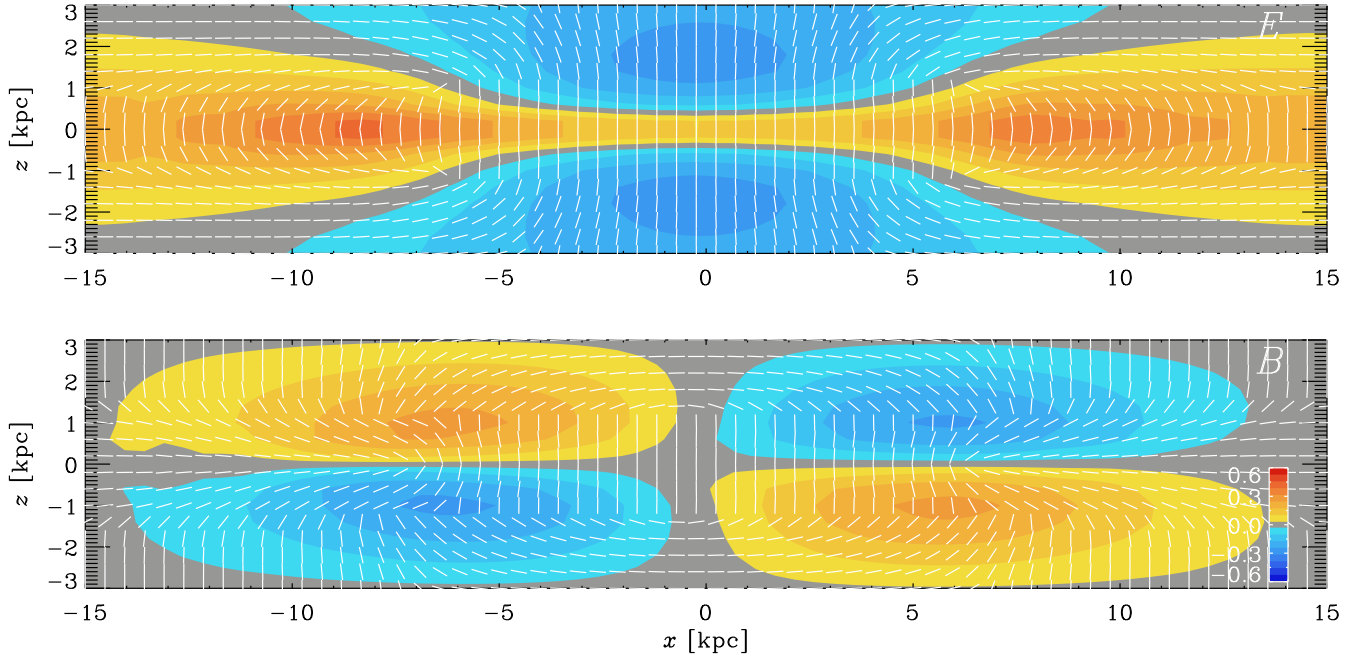


Figure 1. E and B polarizations in an edge-on view of Model A, which is the galactic dynamo model of Brandenburg (2015). The arrow-less vectors show separately the directions of the E and B polarizations, and the color scale shows the values E and B in units where $\epsilon = 1$ in Eq. (3); see (Brandenburg et al. 2019).

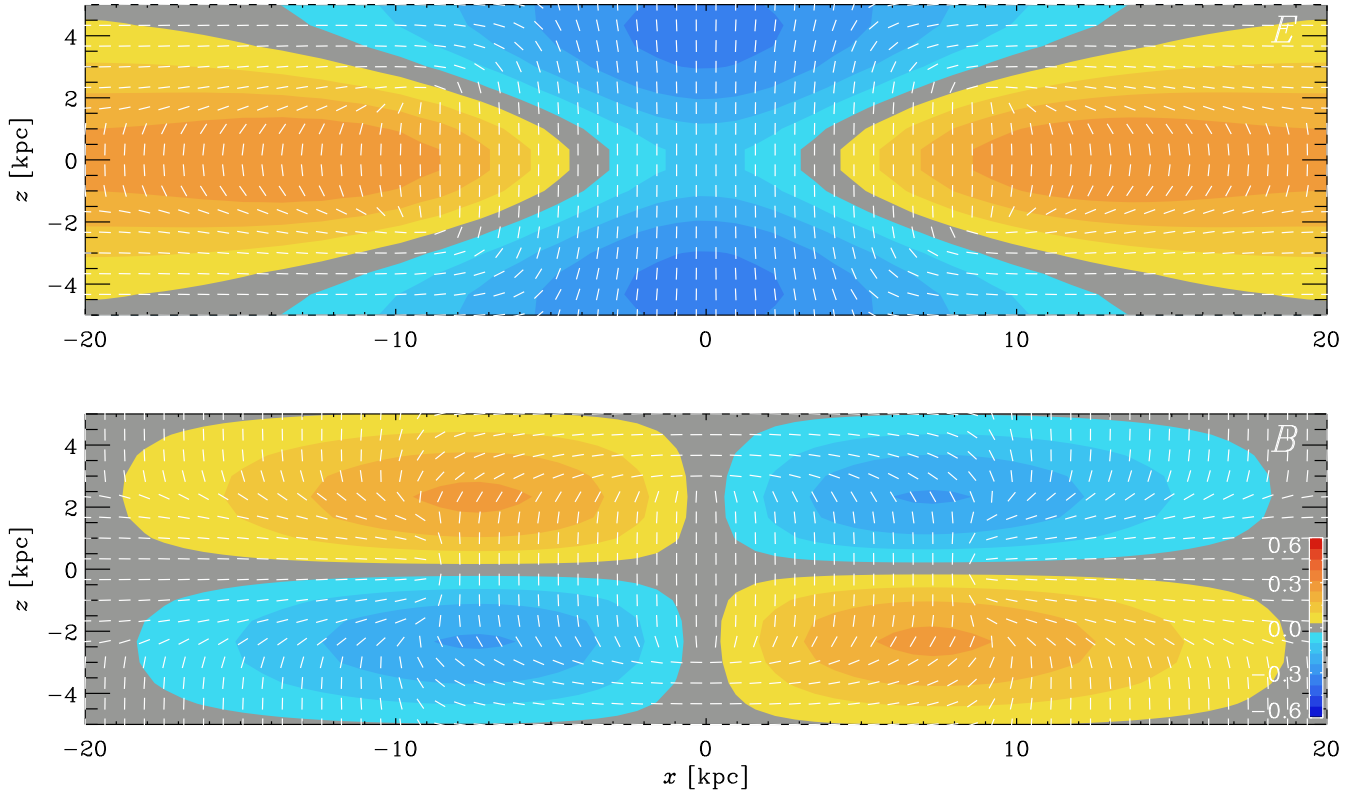


Figure 2. Same as Fig. 1, but for Model B with parameters relevant to NGC 891. Note the pixel resolution of about 650 pc, which corresponds to the 14 arcsecond beam of the JCMT at 850 μ m wavelength.

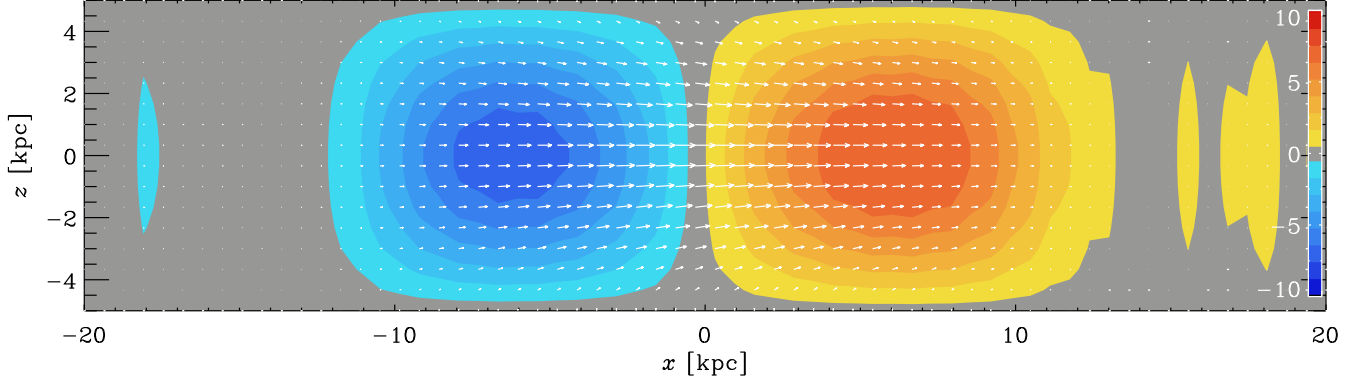


Figure 3. Visualization of the magnetic field for Model B in the same slice for which E and B are shown in Fig. 2. Here, b_z has been scaled by a factor of 20 relative to b_x , but the vertical field still seems almost completely negligible.

formulation (Ivanova & Ruzmaikin 2008) for the horizontal components of the α tensor and choose

$$\alpha_{\perp} = \frac{\alpha_0}{1 + Q_{\alpha} \overline{\mathbf{B}}^2 / B_{\text{eq}}^2} \frac{z}{H_{\alpha}} \exp\left(-\frac{z^2}{H_{\alpha}^2}\right) f_{\alpha}(\varpi), \quad (6)$$

where H_{α} is the disc height for the α effect, α_0 quantifies its strength, and $f_{\alpha}(\varpi)$ is a radial profile that we apply in one of our models. In that case, we use $f_{\alpha}(\varpi) = [1 - \text{erf}(\varpi/\varpi_{\alpha})]/2$. We also define the equipartition field strength as $B_{\text{eq}} = \sqrt{\mu_0 \rho} u_{\text{rms}}$, where u_{rms} is the root-mean-square value of the turbulent velocity. Using $u_{\text{rms}} = 10 \text{ km s}^{-1}$ and $\rho = 2 \times 10^{-24} \text{ g cm}^{-3}$, we have $B_{\text{eq}} = 5 \mu\text{G}$ (Brandenburg et al. 1993), which is the value we use in all of our models. The parameter Q_{α} is a nondimensional constant that determines the strength of α -quenching, and thereby the overall magnetic field strength. We choose $Q_{\alpha} = 25$, so the resulting mean magnetic field strength attains plausible values of somewhat below $10 \mu\text{G}$.

On the periphery of the computational domain, we assume normal-field conditions, i.e., $\hat{\mathbf{n}} \cdot \overline{\mathbf{A}} = (\hat{\mathbf{n}} \cdot \nabla) \times \overline{\mathbf{A}} = 0$. The initial condition for $\overline{\mathbf{A}}(\mathbf{x}, 0)$ is Gaussian distributed white noise of low amplitude. In this paper, we measure lengths in kpc and speeds in km s^{-1} , so time is measured in units of 0.98 Gyr. For simplicity, we drop the factor 0.98 when specifying times or inverse times.

We consider two models. First, we take the one of Brandenburg (2015), which was designed to reflect typical spiral galaxies. Second, we modify the parameters (rotation curve and α effect) such that they match those of the model of Brandenburg et al. (1993) of NGC 891. In both cases, we use $64^2 \times 16$ mesh points, which proved sufficient to resolve the spatial structure of the magnetic field. Calculations with $128^2 \times 32$ mesh points produced virtually identical polarization maps. We emphasize in this connection that we are dealing here with a mean field model, so no sharp structures are expected to occur in such a case. In Table 2 we summarize the various parameters used here. We also give the instantaneous growth rate $\lambda = d \ln B_{\text{rms}} / dt$ during the early exponential growth phase.

Table 2. Parameters of dynamo models A and B.

	Ω_0 [Gyr $^{-1}$]	ϖ_{Ω} [kpc]	α_0 [km s $^{-1}$]	H_{α} [kpc]	ϖ_{α} [kpc]	λ [Gyr $^{-1}$]
A	100	3	16	0.2	—	10
B	75	3	50	1.5	1.0	30

3 RESULTS

Both models lead to an early exponential growth of the magnetic field and reach saturation after about 10 Gyr. Here we consider only the saturated phase of the models. As a first step, we show in Fig. 1 the E and B polarizations for Model A from the xz plane near $y = -10$ kpc. In Fig. 2 we again show the E and B polarizations, but now for Model B. The pixel resolution is about 650 pc, which is the spatial resolution when NGC 891 is observed at a distance of 9.6 Mpc (Strickland et al. 2004) with the 14 arcsecond beam of the James Clerk Maxwell Telescope (JCMT) at $850 \mu\text{m}$ wavelength. We see that, in both cases, E is symmetric about the midplane $z = 0$, and B is antisymmetric. Moreover, E is negative in the halo near the axis ($x = 0$) and positive near the midplane further away from the axis. In Model A, however, E is positive at the center ($x = z = 0$), while in Model B it is negative at $x = z = 0$. As expected, B changes sign about the equator. It also changes sign between the two sides of the rotation axis. In the first and third quadrants, the sign is negative, while in the second and fourth, it is positive. The arrow-less vectors or polarization segments of the B polarization show a clockwise inward swirl in the first and third quadrants and an anti-clockwise inward swirl in the second and fourth quadrants. This signature seems to be surprisingly independent of the differences between Models A and B. The patterns of E and B are surprisingly smooth; the typical scale would be the scale height of the magnetic field, which is about 2 kpc. In this context, we must recall that our model can only deliver the mean magnetic field, and that the actual magnetic field must also contain a fluctuating component of smaller scales below 100 pc.

It is important to realize that neither the helicity of the magnetic field nor any proxy of it can easily be discerned from just a simple inspection of the magnetic field. This is

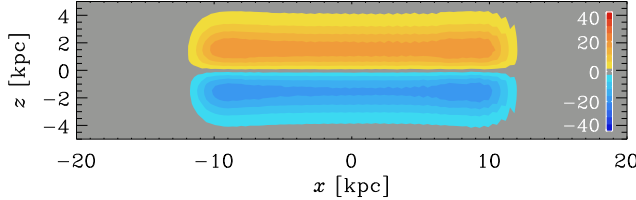


Figure 4. Visualization of the normalized current helicity density, $\mu_0 \mathbf{J} \cdot \mathbf{B}$, for Model B at $y = -10$ kpc.

mostly because of the strong dominance of the azimuthal magnetic field over the vertical field. This becomes clear from Fig. 3, where we show vectors of \mathbf{b}_\perp superimposed on a color scale representation of b_y . Here, b_z has been scaled by a factor of 20 relative to b_x , but the vertical field still seems almost completely negligible.

It is long known that the magnetic field in galaxies tends to have quadrupolar symmetry about the equatorial plane. This is also the case for all of our models. This means that the azimuthal magnetic field is symmetric about the midplane and the vertical magnetic field is antisymmetric about the midplane, just as seen from Fig. 3. Note, also, that the strongest magnetic field occurs at a distance of about 7 kpc from the center. The results for Model A are similar, except that here the strongest magnetic field occurs at a distance of about 5 kpc from the center.

Finally, to make contact with the helicity of the magnetic field in our model, we plot in Fig. 4 a vertical slice of the current helicity density $\mathbf{J} \cdot \mathbf{B}$. We can see that $\mathbf{J} \cdot \mathbf{B}$ is mostly positive (negative) in the upper (lower) disc plane. This agrees with the sign of α_\perp , which is also positive (negative) in the upper (lower) disc plane. For $Q_\alpha = 25$, the normalized current helicity density, $\mu_0 \mathbf{J} \cdot \mathbf{B}$, would be in units of $\mu\text{G}^2 \text{kpc}^{-1}$.

4 DISCUSSION AND FUTURE PROSPECTS

Edge-on galaxies provide an excellent opportunity to study some basic aspects of magnetic fields in galaxies. This has implications for the dynamo interpretation of their generation. Our preliminary investigation suggests that the E polarization is positive near the disc midplane away from the axis, where it tends to outline ring-like patterns, while in the halo near the axis it is negative, corresponding to star-like or expanding patterns; see the top panel of Fig. 1. The B polarization is negative in the first and third quadrants and outlines clockwise inward spiraling patterns, while in the second and fourth quadrants, we have positive values, corresponding to counterclockwise inward spiraling patterns; see the bottom panel of Fig. 1.

Our hope is that the predictions for the signs of the E and B polarizations could soon be verified observationally using observations of dust polarization. Dust polarization observations have proven to be an excellent tool to measure the direction of the magnetic field in star-forming regions and to assess the relative magnitudes of the mean and turbulent components of the field (Hildebrand et al. 2009). Linear polarization imaging provides the orientation of the plane-of-sky B field lines, as non-spherical dust grains tend to align

with their short axis perpendicular to the direction of the magnetic field, giving rise to linear polarization of the emission (Andersson et al. 2015). All-sky dust polarization imaging by *Planck* at 850 μm have revealed well-defined magnetic field field patterns in the interstellar medium of the Milky Way from Galactic scales down to molecular cloud scales of $\gtrsim 10$ pc.

At wavelengths of 850 μm , the optical depth is short and Faraday rotation effects from the superposition along the line-of-sight are limited (Hughes et al. 2014). Intensity maps of NGC 891 at 850 μm show two “blobs” or “knots” at a distance of about 4–5 kpc from the center (Haas et al. 2002; Whaley et al. 2009). This could also be suggestive of a ring-like magnetic field, similarly to what is seen in Fig. 3. This would be analogous to the ring-like magnetic field of M 31 (Beck et al. 2020). Interestingly, the ring-like concentration cannot easily be explained with kinematic theory (Ruzmaikin et al. 1988), unless one invokes a similar variation of the gas density and thereby of B_{eq} (Beck et al. 1996). Such details have been ignored in our present modeling.

A potential shortcoming of the present calculations is that our predictions are based solely on mean-field dynamos. This means that we only take the large-scale component of the magnetic field into account. In reality, there is also a small-scale component whose helicity is expected to have the opposite sign (Blackman & Brandenburg 2003). How this affects the detection prospects of systematic E and B polarizations is currently unknown and must be a target of future investigations. The typical scale of fluctuations would be below 100 pc (Beck et al. 1996), which is well below the resolution scale of the James Clerk Maxwell Telescope. It is therefore possible that our present results may already give a good hint at what can be observed in the near future.

Another opportunity for improvements is given by our increased knowledge of the rotation curves of NGC 891 (Fraternali et al. 2011). In particular, it is now known that the rotation in the halo of NGC 891 is slower than that in the galactic disc (Oosterloo et al. 2007). This implies the presence of vertical shear that could modify the vertical helicity profile of the galaxy.

ACKNOWLEDGEMENTS

This work was supported in part through the Swedish Research Council, grant 2019-04234, and the National Science Foundation under the grant AAG-1615100. We acknowledge the allocation of computing resources provided by the Swedish National Allocations Committee at the Center for Parallel Computers at the Royal Institute of Technology in Stockholm.

REFERENCES

- Alton, P. B., Xilouris, E. M., Misiriotis, A., Dasyra, K. M., & Dumke, M. 2004, *A&A*, 425, 109
- Andersson, B.-G., Lazarian, A., & Vaillancourt, J. E. 2015, *ARA&A*, 53, 501
- Beck, R., Brandenburg, A., Moss, D., Shukurov, A., & Sokoloff, D. 1996, *ARA&A*, 34, 155

Beck, R., Berkhuijsen, E. M., Gießübel, R., & Mulcahy, D. D. 2020, *A&A*, 633, A5

Blackman, E. G., & Brandenburg, A. 2003, *ApJ*, 584, L99

Brandenburg, A. 2015, in *Magnetic fields in diffuse media*, ed. E. de Gouveia Dal Pino & A. Lazarian (Astrophys. Spa. Sci. Lib., Vol. **407**, Springer), 529

Brandenburg, A. 2019, *ApJ*, 883, 119

Brandenburg, A., & Stepanov, R. 2014, *ApJ*, 786, 91

Brandenburg, A., Donner, K. J., Moss, D., Shukurov, A., Sokoloff, D. D., & Tuominen, I. 1993, *A&A*, 271, 36

Brandenburg, A., Bracco, A., Kahniashvili, T., Mandal, S., Roper Pol, A., Petrie, G. J. D., & Singh, N. K. 2019, *ApJ*, 870, 87

Durrer, R. 2008, *The Cosmic Microwave Background* (Cambridge: Cambridge University Press)

Fraternali, F., Sancisi, R., & Kamphuis, P. 2011, *A&A*, 531, A64

Haas, M., Klaas, U., & Bianchi, S. 2002, *A&A*, 385, L23

Hildebrand, R. H., Kirby, L., Dotson, J. L., Houde, M., & Vaillancourt, J. E. 2009, *ApJ*, 696, 567

Horellou, C., & Fletcher, A. 2014, *MNRAS*, 441, 2049

Hughes, T. M., Baes, M., Fritz, J., Smith, M. W. L., Parkin, T. J., et al. 2014, *A&A*, 565, A4

Ivanova, T. S., & Ruzmaikin, A. A. 1977, *Sov. Astron.*, 21, 479

Junklewitz, H., & Enßlin, T. A. 2011, *A&A*, 530, A88

Kahniashvili, T., Maravin, Y., Lavrelashvili, G., & Kosowsky, A. 2014, *PhRvD*, 90, 083004

Kamionkowski, M., & Kovetz, E. D. 2016, *ARA&A*, 54, 227

Kamionkowski, M., Kosowsky, A., & Stebbins, A. 1997, *PhRvL*, 78, 2058

Krause, F., & Rädler, K.-H. 1980, *Mean-field Magnetohydrodynamics and Dynamo Theory* (Oxford: Pergamon Press)

Oosterloo, T., Fraternali, F., & Sancisi, R. 2007, *ApJ*, 134, 1019

Oppermann, N., Junklewitz, H., Robbers, G., & Enßlin, T. A. 2011, *A&A*, 530, A89

Parker, E. N. 1955, *ApJ*, 122, 293

Parker, E. N. 1971, *ApJ*, 163, 255

Planck Collaboration Int. XIX. 2015, *A&A*, 576, A104

Prabhu, A., Brandenburg, A., Käpylä, M. J., & Lagg, A. 2020, *A&A*, submitted, arXiv:2001.10884

Rüdiger, G. 1978, *Astron. Nachr.*, 299, 217

Ruzmaikin, A. A., Sokoloff, D. D. & Shukurov, A. M. 1988, *Magnetic Fields of Galaxies* (Kluwer, Dordrecht)

Seljak, U., & Zaldarriaga, M. 1997, *PhRvL*, 78, 2054

Shukurov, A. 1998, *MNRAS*, 299, L21

Steenbeck, M., Krause, F., & Rädler, K.-H. 1966, *Z. Naturforsch.*, 21a, 369

Strickland, D. K., Heckman, T. M., Colbert, E. J. M., Hoopes, C. G., & Weaver, K. A. 2004, *ApJ*, 606, 829

Vainshtein, S. I., & Ruzmaikin, A. A. 1971, *Sov. Astron.*, 16, 365

Volegová, A. A., & Stepanov, R. A. 2010, *Sov. Phys. JETP*, 90, 637

Whaley, C. H., Irwin, J. A., Madden, S. C., Galliano, F., & Bendo, G. J. 2009, *MNRAS*, 395, 97